

Improving Feature-based Visual Localization by Geometry-Aided Matching

Hailin Yu, Youji Feng, Weicai Ye, Mingxuan Jiang, Hujun Bao, Guofeng Zhang

Abstract—Feature matching is an essential step in visual localization, where the accuracy of camera pose is mainly determined by the established 2D-3D correspondence. Due to the noise, solving the camera pose accurately requires a sufficient number of well-distributed 2D-3D correspondences. Existing 2D-3D feature matching is typically achieved by finding the nearest neighbors in the feature space, and then removing the outliers by some hand-crafted heuristics. However, this may lead to a large number of potentially true matches being missed or the established correct matches being filtered out. In this work, we introduce a novel 2D-3D matching method, Geometry-Aided Matching (GAM), which uses both appearance information and geometric context to improve 2D-3D feature matching. GAM can greatly strengthen the recall of 2D-3D matches while maintaining high precision. We insert GAM into a hierarchical visual localization pipeline and show that GAM can effectively improve the robustness and accuracy of localization. Extensive experiments show that GAM can find more correct matches than hand-crafted heuristics and learning baselines. Our proposed localization method achieves state-of-the-art results on multiple visual localization datasets. Experiments on Cambridge Landmarks dataset show that our method outperforms the existing state-of-the-art methods and is six times faster than the top-performed method. The source code is available at <https://github.com/openxrlab/xrlocalization>.

Index Terms—Visual Localization, Relocalization, Feature Matching, Augmented Reality

1 INTRODUCTION

VISUAL localization aims to estimate the 6-Degree-of-Freedom (6DoF) camera pose from a single image, which is a fundamental technique for many applications, such as augmented reality, autonomous driving, and mobile robotics.

Feature-based visual localization methods [1], [2], [3], [4], [5], [6], [7], [8] mainly follow a classic four-stage pipeline: 1) extracting local features (keypoints and descriptors), 2) establishing 2D-3D correspondences by performing feature matching between a query image and an offline reconstructed SfM model, 3) estimating the camera pose by solving a standard PnP [9], [10] inside a RANSAC [11] loop, 4) refining the camera pose with all inliers. In this pipeline, a key step for accurate and robust localization is to find a sufficient number of correct 2D-3D correspondences due to the existence of noise and mismatches.

SIFT [12] is the widely used local feature in this pipeline. While performing well in normal circumstances, it is less effective in scenes with illumination or large viewpoint changes [1]. One way to deal with this issue is to enhance the discriminative power of local features used in this pipeline. Recently, a large number of CNN-based local features have also been proposed. They use deep networks to extract descriptors solely [13], [14], [15], [16] or extract keypoints and descriptors simultaneously [17], [18]. These features show impressive robustness against illumination variations and viewpoint changes and perform better than hand-crafted

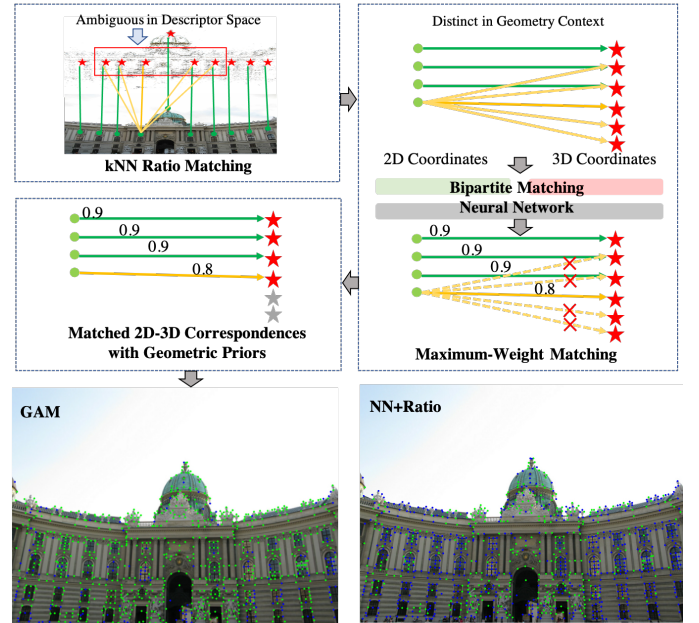


Fig. 1. **Geometry-Aided Matching**. The above part is the illustration of GAM. The below part is two query images matched by GAM and NN matcher followed by ratio test, respectively. Green dots are 2D points that are matched with 3D points correctly. Blue dots are unmatched or wrong matched 2D points.

ones on feature matching. Some of them have already been used to improve localization [1], [18]. However, if feature matching is performed by finding the nearest neighbor (NN) in descriptor space, a large number of potential true matches may still be lost due to the intrinsically limited invariance and discriminative power of local features, even with the

• H. Yu, W. Ye, H. Bao and G. Zhang are with the State Key Lab of CAD&CG, Zhejiang University, and also affiliated with ZJU-SenseTime Joint Lab of 3D Vision. E-mails: hailinyu0414@gmail.com, [yeweicai, bao-hujun, zhangguofeng}@zju.edu.cn](mailto:{yeweicai, bao-hujun, zhangguofeng}@zju.edu.cn). H. Yu is also affiliated with SenseTime Research. G. Zhang is the corresponding author.

• Y. Feng and M. Jiang are with SenseTime Research.

powerful learning-based ones. The number of true matches will be further reduced by performing the ratio test that is commonly used to reject ambiguous matches, especially when repetitive patterns exist in scenes.

Recent works [19], [20], [21] propose to use a neural network to learn a function to classify inliers and outliers or to predict matching probability or directly to learn a match function [22] for 2D image matching. These data-driven methods show promising results on 2D-2D feature matching. However, the widely used method for 2D-3D matching is still to find the nearest neighbor and followed by ratio test [1], [7], [12], or some heuristic methods [2], [4]. Some recent methods [1], [22] establish 2D-3D correspondences by performing 2D-2D matching between the query image and all retrieved reference images. When localizing the query images, multiple 2D-2D feature matching is required as many times as the number of retrieved images. This is very time-consuming and usually takes several seconds to obtain accurate poses. Therefore, this type of approach is not well suited to eliminate tracking drift in AR applications timely.

To address the problem aforementioned, we propose a geometry-aided matching (GAM) method, which directly matches 2D features in the query image to 3D points in the SfM model. The descriptor of a 3D point can be represented by the mean of all 2D descriptors in the track. GAM is a two-step matching method. As shown in Fig.1, all potential true matches are firstly found by k NN ratio matching as candidates, which can recall the correct matches that are not in the nearest neighbor. As a price, this brings a large number of outliers. For each 2D feature, there may be k incorrect matches. To solve this problem, we turn to leverage the geometric information to find true matches from these candidates, based on the observation that some matches are ambiguous in feature space but distinct in geometry context [15], [19]. Inspired by [19], we propose a deep neural network to learn the geometric context from candidate matches and then use geometric information to reject outliers. Unlike [19] which treats all 2D-2D correspondences as a 4D point set, we instead view 2D-3D correspondences as three sets, i.e., 2D point set, 3D point set, and edge sets, then use three networks to process these sets separately. This approach can effectively reuse the features extracted from 2D and 3D point sets. In addition, to find the globally optimal one-to-one matches from one-to-many candidates, we introduce a Hungarian pooling layer to ensure that the output of the network is one-to-one matches, so we call the network bipartite matching neural network (BMNet). Moreover, this pooling layer can effectively avoid the geometrically consistent mismatching problem.

To cope with large scenes, we embed GAM into a hierarchical visual localization pipeline. Based on the retrieved images, a scene retrieval strategy is proposed to expand the retrieval result exploiting co-visible information provided by the SfM model. This strategy can provide a more complete set of matches for 3D points. Compared to our prior work [23], we make several modifications to improve robustness. Specifically, we propose a novel k NN ratio matching to replace k NN matching, which not only improve the quality of matching candidates but also make it less sensitive to the hyper parameter k . We also improve the discriminative power of BMNet by adopting a new

method to generate training data. To summarize, our major contributions are as follows:

- We propose GAM that firstly establishes multiple candidate matches for each 2D point depend on visual appearance and then filter incorrect matches depend on geometric context.
- We propose a deep neural network, referred to BMNet, to deal with many-to-many candidate matches. It can predict the geometric prior of each 2D-3D match and output the globally optimal match set.
- We propose a hierarchical visual localization method with a new scene retrieval strategy, which further improves the robustness of pose estimation.
- We show that the proposed localization method outperforms the state-of-the-art methods on multiple datasets.

The rest of the paper is organized as follows. Related work is discussed in Section 2. The proposed matching method and neural network are described in Section 3. The whole localization pipeline is presented in Section 4. In Section 5, we conduct extensive experiments to justify our proposed method and compare it to the state-of-the-art methods.

2 RELATED WORK

Visual localization involves many fields, such as local feature, feature matching, and pose estimation. In this section, we briefly review some methods related to our work.

Local Feature. Traditional hand-crafted local features [12], [24] are sensitive to illumination variation and large viewpoint changes. When the scene lighting changes, it is difficult to find a sufficient number of correct matches. Recently, many CNN-based local features [13], [14], [15], [16], [17], [18] are proposed to replace hand-crafted ones and show a better result on image matching and visual localization [1], [18]. However, there are many similar local patterns in real environments, e.g. the facades of modern buildings. Ambiguous matches would be frequently encountered even using powerful learning-based features. The problem can be alleviated by embedding some contextual information from the whole image in the features [13], [15], but this will obscure the raw representation of local details.

Feature Matching. Feature matching typically takes two steps: 1) establishing initial matches through the Nearest Neighbor (NN) search, 2) filtering ambiguous matches by some strategies, such as ratio test [12], distance threshold, and cross check. In addition to these simple and general strategies, for the problem of image matching, some works [25], [26] leverages local consistency and uses neighborhood consensus to gather correct matches and remove mismatches. If a geometric model, e.g. a fundamental matrix or an absolute pose, fits for the true matches, robust model estimation approaches can be used to find out the inliers, such as [11], [27], [28], [29]. Recently, some methods [19], [20] propose to use a deep neural network to classify initial matches as inliers or outliers, or directly predict the probability of matching [30]. They have shown impressive results on 2D-2D image matching. NCNet [31] develops an end-to-end trainable convolutional neural network architecture

that identifies sets of spatially consistent matches by analyzing neighborhood consensus patterns. Feature matching can also be formulated as graph matching, which aims to establish correspondences between two graphs. It is usually formulated as a quadratic assignment problem that is NP-hard. For a bipartite graph, if the candidate matches and the corresponding weights are given, some methods [32], [33] can find the global optimal solution with the maximum sum of weights. Recent works show that graph matching can also be solved by learning methods. [34] is the first work to leverage learning to accelerate the matching process. [35] uses deep architecture to improve performance. SuperGlue [22], parallel to our prior work [23], designs a graph neural network for feature matching and uses self-attention and cross-attention to aggregate global context to achieve robust matching. [36] adopts a coarse-to-fine manner to accelerate feature matching. OnePose [37] proposes an architecture based on a graph attention network for 2D-3D feature matching, but it only works on object-level pose estimation and can not apply to large-scale visual localization.

Feature-based Localization. Feature-based visual localization mainly relies on feature matching between a query image and an offline reconstructed map to get 2D-3D correspondences. In the past, many methods [2], [3], [4], [5], [6], [38], [39] performs direct matching between local features in a query image and the 3D points in an SfM model. As the feature set in the database is typically very large, many previous works aim to improve efficiency. [39] uses a large vocabulary to quantize the local features and prefers to match the features with lower cost in priority. [5] compresses the 3D model and ranks the 3D points according to the chances they might be seen. Direct matching may produce many false correspondences, some methods [2], [4], [38] use the constrain of co-visibility to obtain positive matches. To cope with large-scale scenarios, some methods adopt a hierarchical paradigm. Image global features [40], [41] are firstly extracted to perform image retrieval to find the similar images in the database and then match the query features with the points visible in the retrieved images. These methods are more robust if a superior image retrieval method [40] is provided, and easy to integrate with some location prior. Apart from the low-level local features, some approaches [42], [43], [44] also use the high-level semantic information to improve the robustness against seasonal changes or extreme illumination changes. Recently, some methods get 2D-3D correspondences by performing 2D-2D feature matching between a query image with multiple retrieved database images, which is time-consuming and required large storage to store all local features. Different from these methods, our method directly matches the 2D query features with the 3D points, each 3D point may store only one descriptor.

End-to-End Localization. End-to-End localization methods can be classified as either directly regressing the camera pose [45], [46], [47], [48], [49] or regressing scene coordinates [50], [51], [52], [53]. They do not suffer from the problems of local feature matching and are very robust under the scenes with illumination changes or texture-less regions. PoseNet [47] is the first work that proposes to train a the convolutional neural network to directly regress the 6DoF pose from a given query image. Based on this pioneering

work, many improvements on the accuracy are achieved through the novel design of network architectures or loss functions [45], [46]. These pose regression methods behave more like image retrieval [54], thus the accuracy is unsatisfactory, especially for various AR applications. Another type of learning-based method [50], [51], [52] firstly regress the scene coordinates of the query image and then compute the camera pose using the PnP algorithm. SCoRe Forest [50] uses the regression forest to infer the coordinates of each pixel in the RGB-D image and then uses RANSAC+PnP to solve the camera pose. DSAC [51] proposed a differentiable RANSAC to train this process in an end-to-end way. [52] further improves the accuracy through a fully convolutional neural network for densely regressing scene coordinates. These methods are more accurate than direct pose regression but are hard to converge in large-scale scenarios. Besides, the generalization ability of the learning-based method remains a knotty problem, the requirement of a large amount of training data limits their scalability and applications. PixLoc [55] also adopts an end-to-end manner but it casts camera localization as metric learning and exhibits exceptional generalization to new scenes by separating model parameters and scene geometry. Different from these end-to-end methods, GAM focus on 2D-3D feature matching and is learned separately not embedded in the whole complicated localization pipeline.

3 GEOMETRY-AIDED MATCHING

In this section, we describe the proposed 2D-3D matching method GAM. We first present the problem formulation and describe BMNet architecture and finally describe training BMNet using SfM models. The details are presented below.

3.1 Problem Formulation

Given two feature sets, \mathcal{A} and \mathcal{B} , to be matched, $\mathcal{A} = \{f_1^a, \dots, f_M^a\}$ is 2D feature set and $\mathcal{B} = \{f_1^b, \dots, f_N^b\}$ is 3D feature set. We denote feature as $f_i = (p_i, d_i)$, where p_i is coordinate (x_i, y_i) for the 2D feature set \mathcal{A} and (X_i, Y_i, Z_i) for the 3D feature set \mathcal{B} . $d_i \in \mathbb{R}^D$ is the descriptor that can be extracted using SuperPoint [17] or other local features such as D2Net [18]. Each 3D point descriptor d_i is represented by the mean of all descriptors in the track.

We first introduce k NN ratio matching to establish 2D-3D correspondences with similar appearance. Specifically, for 2D feature f_i^a , K nearest 3D points in descriptor space are firstly found as initial matches $\{m_{i1}, \dots, m_{iK}\}$, which distances are denoted as d_{i1}, \dots, d_{iK} and satisfy $d_{i1} < \dots < d_{iK}$. Then, the matches that satisfy $d_{i1}/d_{ik} \geq r$ are selected as candidates, where k is from 2 to K and r is the ratio threshold. If $r = 1$, it equals to finding the nearest neighbor, and if $r = 0$, it equals to find the K nearest neighbors.

BMNet is then introduced to filter outliers from candidate matches by leveraging geometric context. We view these candidate matches and corresponding 2D and 3D points as a bipartite graph denoted as $\mathcal{G} = (\mathcal{U}, \mathcal{V}, \mathcal{E})$. $\mathcal{U} = \{p_1^a, \dots, p_M^a\}$ is the 2D point set that constructed by all matched 2D points. $\mathcal{V} = \{p_1^b, \dots, p_N^b\}$ is the 3D point set that constructed by all matched 3D points. $\mathcal{E} = \{e_1, e_2, \dots, e_T\}$ is the edge set, where each edge $e_k = (i, j)$ with $1 \leq k \leq T$

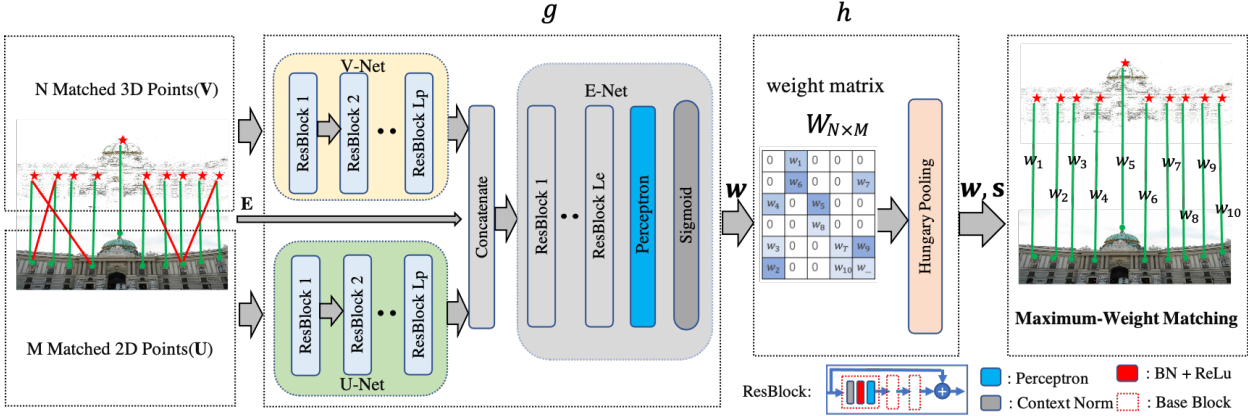


Fig. 2. **BMNet Architecture.** BMNet takes a bipartite graph as input and outputs the maximum-weight matching and the corresponding probability of being an inlier for each selected correspondence. The input graph is composed of the 2D point set (\mathcal{U}), the 3D point set (\mathcal{V}), and the 2D-3D correspondence set (\mathcal{E}) in which the inliers are displayed in green and the outliers are displayed in red. Three sub-networks (U-Net, V-Net, and E-Net) are used to extract the geometric features for \mathcal{U} , \mathcal{V} , and \mathcal{E} respectively.

represents that there is a match between the i -th 2D point and the j -th 3D point. T is the number of all candidate matches. BMNet aims to predict a weight w_k for each edge e_k and then find the maximum-weight matching \mathcal{M} , which is a subset of \mathcal{E} . The weight w_k represents the likelihood that e_k is an inlier. The outputs of BMNet are formally written as a weighting vector $\mathbf{w} = (w_1, w_2, \dots, w_T)$ with $w_k \in [0, 1]$ and an assignment vector $\mathbf{s} = (s_1, s_2, \dots, s_T)$ with $s_k \in \{0, 1\}$ which indicates whether the k -th edge is contained in the maximum-weight matching \mathcal{M} .

Finally, GAM selects the edges with $s_k = 1$ as final matches, which are used to solve camera pose. The architecture of BMNet is elaborated in the next section.

3.2 Network Architecture

This part describes the proposed deep architecture BMNet. The overall architecture is illustrated in Fig.2. The input is a bipartite graph \mathcal{G} constructed from the 2D-3D correspondences established by k NN ratio matching. The workflow of BMNet can be divided into two steps. The first step is to predict weighing vector $\mathbf{w} = g(\mathcal{G}; \theta)$, where θ is the learning parameters. The second step is to find out the maximum-weight matching result from \mathcal{G} and \mathbf{w} , denoted as $\mathbf{s} = h(\mathcal{G}, \mathbf{w})$, where the function h is non-parametric. The final output is obtained by combining the above two parts, denoted as:

$$(\mathbf{w}, \mathbf{s}) = f_{\theta}(\mathcal{G}) \quad (1)$$

Since the three parts, i.e. the two point sets \mathcal{U} and \mathcal{V} , and the edge set \mathcal{E} , of the bipartite graph, are all unordered sets, we use Perceptron [56] as the basic layers to extract the geometric features and use Context Normalization [19] to aggregate the global information.

As shown in Fig.2, $g(\mathcal{G}; \theta)$ contains three sub-networks, represented by U-Net, V-Net, and E-Net, respectively. The input to U-Net is the 2D point set \mathcal{U} , which can be represented as a $M \times 2$ matrix. U-Net embeds the M 2D point coordinates into $M d_1$ -dimensional vectors, so the output of U-Net is a $M \times d_1$ matrix \mathbf{X}_u . Similarly, the input to V-Net is the 3D point set \mathcal{V} , which can be represented as a $N \times$

matrix. V-Net embeds the N 3D point coordinates into $N d_2$ -dimensional vectors, and the output of V-Net is a $N \times d_2$ matrix \mathbf{X}_v . According to the edge set \mathcal{E} , we concatenate the corresponding 2D and 3D feature vectors to form the input to E-Net \mathbf{X}_e , which is a $T \times (d_1 + d_2)$ matrix. In this work, both d_1 and d_2 are set to 128. For a specific edge $e_k = (i, j)$, the feature vector input to E-Net can be obtained by:

$$\mathbf{X}_e^k = [\mathbf{X}_u^i \parallel \mathbf{X}_v^j], \quad (2)$$

where \mathbf{X}_*^r denotes the r -th row of matrix \mathbf{X}_* and $[\cdot \parallel \cdot]$ denotes concatenation. The output of E-Net is a T -dimensional vector and a sigmoid layer on the top of E-Net is used to ensure that each value of the output vector \mathbf{w} is in the range of $[0, 1]$.

Hungarian Pooling. If we train $g(\mathcal{G}; \theta)$ directly, the network parameters will be very difficult to learn because the geometric consistency may conflict with the supervision. The conflict is shown in Fig.3. A 2D image point is matched with two 3D points being close in 3D space. They may both have small reprojection errors with the same camera pose. The network is prone to generate similar weights for them according to the extracted geometric features. These two correspondences are considered geometric consistent. However, only one of them may be an inlier and the rest is an outlier. This discrepancy that the multiple correspondences have similar geometric features but with different labels makes the network hard to converge.

To solve this problem, we introduce the Hungarian algorithm [33] into the network for end-to-end training. Hungarian algorithm can find the global optimal one-to-one matches. Because only one of the two correspondences is selected, the discrepancy between the geometric consistency and the supervision can be eliminated.

Based on the weight vector \mathbf{w} predicted by $g(\mathcal{G}; \theta)$ and the bipartite graph \mathcal{G} , a weight matrix \mathbf{W} is constructed as:

$$\mathbf{W}[e_k[0], e_k[1]] \leftarrow w_k, \quad (3)$$

where the unfilled elements of \mathbf{W} is set to 0. Then the Hungarian algorithm is applied on this weight matrix \mathbf{W}

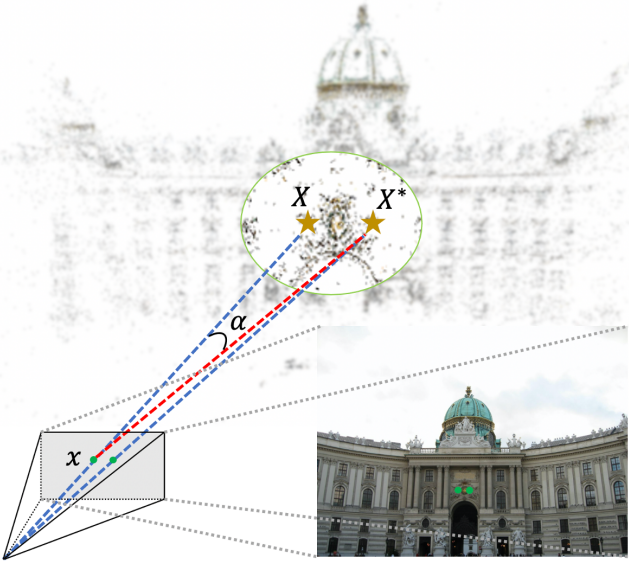


Fig. 3. X and X^* are two 3D points, and x is the projection of X on the image plane. The correspondence (X^*, x) is an outlier established by feature matching. (X, x) is the correct match. When the angle α is small, two correspondences (X^*, x) and (X, x) should have similar weights from a geometric view, but from a learning view, the weight of correspondence (X^*, x) should be much smaller than correspondences (X, x) due to their respective label. This produces a conflict that makes the network hard to train.

to get the maximum-weight matching \mathcal{M} . The assignment vector s is obtained by

$$s_k = \begin{cases} 1 & e_k \in \mathcal{M}; \\ 0 & \text{otherwise.} \end{cases} \quad (4)$$

Since the output edges come from a subset of the input edges, the layer introducing the Hungarian algorithm can be regarded as a special sampling layer, which we referred to as the Hungarian pooling. The back-propagation used in the end-to-end training is formulated as:

$$\frac{\partial h(\mathcal{G}, \mathbf{w})}{\partial w_k} = \begin{cases} 1 & e_k \in \mathcal{M}; \\ 0 & \text{otherwise.} \end{cases} \quad (5)$$

3.3 Learning from SfM Model

In this section, we describe how to learn the parameters of BMNet. There are three parts: 1) training data generation, 2) data augmentation, and 3) the loss function.

Training Data Generation. The training data can be generated automatically using the SfM technique. We generate a bipartite graph for each image that has been registered by SfM. Specifically, for an image I in the SfM model, we take the extracted 2D keypoints and their corresponding descriptors to form the 2D feature set. Then, all the 3D points observed by the images that are co-visible with image I and its corresponding descriptors are used to form the 3D feature set. The descriptor of each 3D point is represented as the mean of all 2D descriptors in the track except in image I . The edge set is generated online at the training stage.

Negative Sample Mining. Different from the previous work [23] where all negative edges are generated in a

completely random manner, we instead perform k NN ratio matching online with a fixed number of randomly selected features from both 2D and 3D feature sets to generate positive and negative edge samples during training. The negative samples generated in this way tend to be harder than that of random selection while being consistent with the inference stage in terms of data distribution. This can effectively improve the discriminative power of the training model.

Loss Function. Finding true matches from the candidates is essentially a classification problem, so we use the widely used cross-entropy loss function for training:

$$\mathcal{L}_{\theta} = \frac{1}{T} \sum_{k=1}^T (t_k \log(w_k) s_k + (1 - t_k) \log(1 - w_k) s_k). \quad (6)$$

where $t_k = 1$ is for true match otherwise $t_k = 0$.

4 HIERARCHICAL VISUAL LOCALIZATION

In this section, we embed the proposed geometry-aided matching method (GAM) into a hierarchical visual localization pipeline, shown in Fig.4. For a query image, its global feature and local features are extracted. The global feature is used for coarse localization to determine the 3D point set to be matched. Both the extracted local features and the 3D point set combining corresponding descriptors are fed into GAM to get global optimal 2D-3D correspondences. The whole localization process is divided into three modules namely scene retrieval, 2D-3D feature matching, and prior-guided pose estimation. The following describes these modules in detail.

Scene Retrieval. We define a set of the 3D points observed in one image in an SfM model as a meta scene, so we can get a set of the meta scenes $\mathcal{S} = \{S_1, S_2, \dots, S_N\}$ from a given SfM model, where N is the number of registered images. We use the global descriptor of the query image to retrieve the top R images $\mathcal{I} = \{I_1, I_2, \dots, I_R\}$ from the database. The corresponding meta scenes are denoted as $\hat{\mathcal{S}} = \{\hat{S}_1, \hat{S}_2, \dots, \hat{S}_R\}$. Instead of directly using the meta scenes for feature matching, we further perform an expansion. We denote $\beta = |S_i \cap S_j|$, which is the number of co-visible 3D points of two scenes. $\beta > 0$ means that the meta scenes S_i and S_j are co-visible. For each retrieved meta scene \hat{S}_i in $\hat{\mathcal{S}}$, we expand it according to co-visibility. This is achieved by finding all meta scenes from \mathcal{S} that are co-visible with \hat{S}_i and then selecting the top m ones with the most co-visible points. Then, all the selected m meta scenes are merged as an expanded scene \hat{S}_k . The expansion is performed for the retrieved meta scenes in descending order according to the retrieval scores. If the next retrieved meta scene has already appeared in the previous scenes, we simply skip it. Finally, we get a set of scenes $\bar{\mathcal{S}} = \{\bar{S}_1, \bar{S}_2, \dots, \bar{S}_K\}$, which will be used for local feature matching.

2D-3D Feature Matching. GAM is performed sequentially according to the order of the scene retrieval and outputs matched 2D-3D correspondences. For the k -th scene \bar{S}_k , we fetch its 3D points and corresponding descriptors to construct the 3D feature set. GAM is performed between the 2D local features extracted from the query image and the 3D

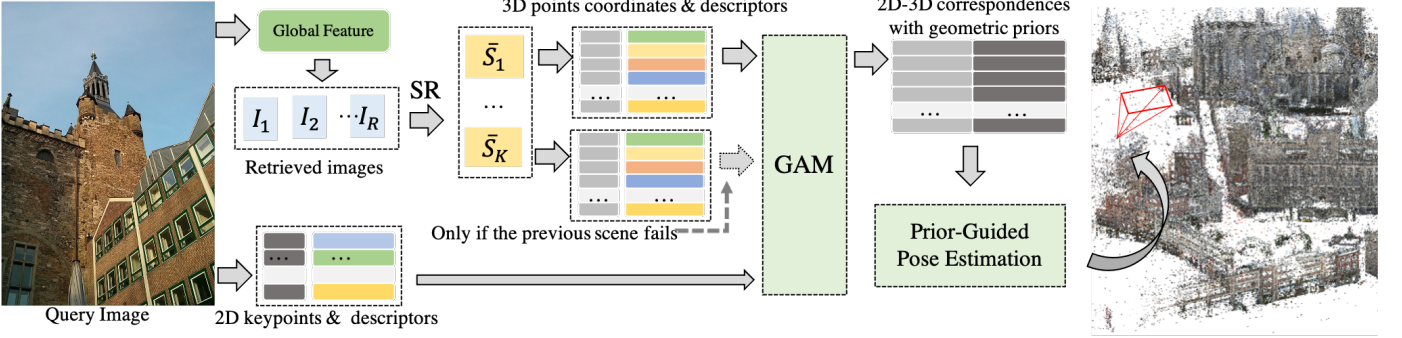


Fig. 4. **Hierarchical Visual Localization Pipeline.** GAM is embedded in a hierarchical visual localization pipeline with scene retrieval strategy. Global and local features are extracted from a query image and are used for scene retrieval and 2D-3D feature matching (GAM). Finally, prior-guided pose estimation is performed depending on the output of GAM.

feature set and outputs the maximum-weight matching \mathcal{M} . We perform k NN ratio matching depending on Euclidean distances, which can be achieved efficiently through matrix operations when descriptors are normalized.

Prior-Guided Pose Estimation. Since there are still some false matches in \mathcal{M} , we apply a PnP solver inside the RANSAC loop. In the RANSAC loop, the probability of sampling 2D-3D correspondences is decided by the likelihood predicted by BMNet. This allows us to sample possible inliers with larger chances.

Our pipeline is partially inspired by the current state-of-the-art method [1]. It clusters the retrieved images to form several scenes by using co-visibility. The fine localization is performed against each scene in descending order according to the size of the scene. The localization is terminated if a credible result, e.g. the number of inliers is larger than a threshold, is obtained. We use the same early-stop strategy, but the construction of the scene is different. First, the scene in [1] contains the retrieved images only, we make an expansion in the original SfM model to effectively find more relevant 3D points. Second, the clustering in [1] uses an unlimited transitive co-visibility. This may gather many images that are far away from each other and of which most of the scenes are indeed different. Many outliers may be produced when performing feature matching with the scene. Instead, we limit the size of the scene and prefer the non-transitive co-visibility to get a cleaner scene.

The proposed localization method is not limited to a specific image retrieval method and a specific local feature. In this work, if not otherwise specified, we use NetVLAD [40] and SuperPoint [17] as the global and local feature extractors, respectively.

5 EXPERIMENTS

In this section, we verify the effectiveness of the proposed 2D-3D matching method GAM through extensive experiments and demonstrate the state-of-the-art localization performance on multiple public datasets. We first discuss the architecture details and our training configuration. Then, we evaluate GAM and the proposed localization method. Finally, we compare our method with state-of-the-art methods and provide an ablation study.

5.1 Architecture Details and Training Setup

The number of blocks of U-Net and V-Net L_p and E-Net L_e is set to 5 and 18, respectively. The model is implemented in PyTorch [57]. We use MegaDepth dataset [58], which includes 196 different locations. Each location provides an SfM model reconstructed by COLMAP [59] using SIFT. We select four locations, which include about 12k images. We fix all image poses and use HLoc toolbox [22], [60] to reconstruct the selected 4 locations with SuperPoint. We use the reconstructed SfM models to construct our training set. If not otherwise specified, all learned methods used in the following experiments are trained under this training set. BMNet used in GAM is trained using an SGD optimizer with an initial learning rate 0.001 and batch size 1. It converges after 140 epochs of training on one GTX1080Ti GPU. The following experiments, if not otherwise specified, use GAM with $k = 3$ and $ratio = 0.7$ as the default configuration.

5.2 2D-3D Matching

We first perform 2D-3D matching experiments and show that GAM can find more true matches with higher precision than hand-crafted methods and learning methods.

Dataset. We choose one location from MegaDepth dataset [58] as the test dataset for 2D-3D matching evaluation. The chosen location is totally different from the training set. The dataset includes 508 images. We fix all image poses and use HLoc toolbox [22], [60] to reconstruct this location with SuperPoint [17].

Metrics. We report match precision and match recall, which are computed from the ground truth 2D-3D correspondences. Match precision refers to the ratio of ground truth correspondences being matched over the number of all matches. Match recall refers to the ratio of true correspondences being matched over the number of all true correspondences. We further use matched 2D-3D correspondences to compute the poses for all test images and report the median positional errors (MPE, no scale) and the median rotation errors (MRE, $^\circ$) for evaluating of the accuracy of estimated poses.

Compared with Baselines. We compare GAM with both traditional hand-crafted methods and learned matching methods. All methods use SuperPoint feature. For all

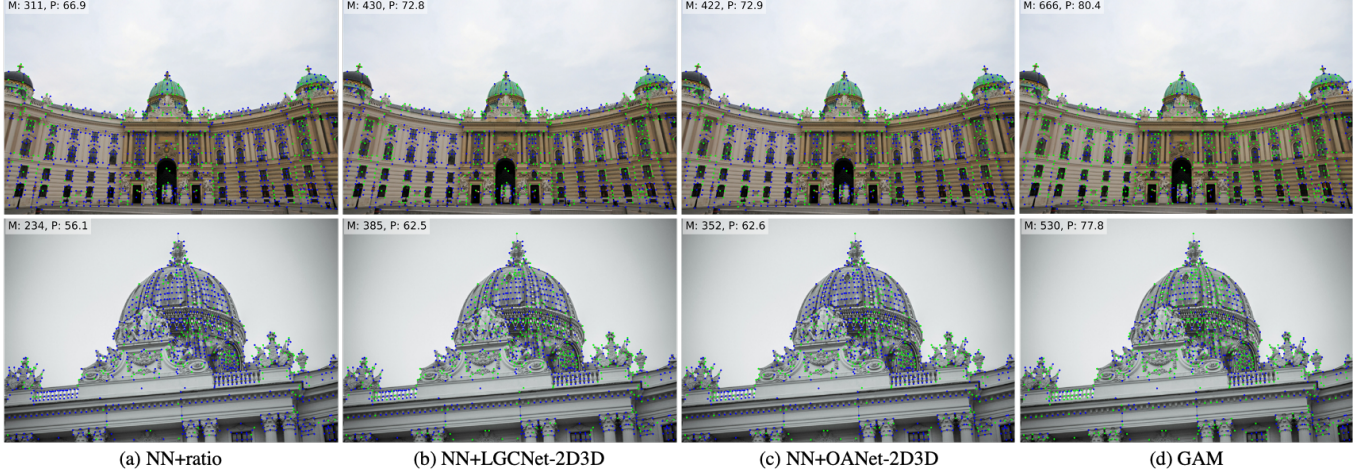


Fig. 5. **Qualitative 2D-3D matching.** Blue dots and green dots represent unmatched keypoints and truly matched keypoints, respectively. M and P represents the number of correct matches and the match precision, respectively.

baselines, we use the Nearest Neighbor (NN) matcher, finding the nearest neighbor from all 3D points for each 2D point in the descriptor space. The hand-crafted outlier rejection methods include ratio test (ratio), distance threshold (distance), and being the nearest neighbors to each other (cross check). OnePose [37] only works on object-level 2D-3D feature matching and can not handle feature matching in such large-scale scenes. Except for OnePose, there is no other learning-based method directly used for 2D-3D feature matching. Therefore, we migrate some of the recently proposed methods that perform well in 2D-2D matching to 2D-3D for comparison. We replace the input of LGCNet [19] and OANet [20] from 2D-2D correspondences to 2D-3D correspondences, namely LGCNet-2D3D and OANet-2D3D respectively. The training method is kept the same as BMNet. We try to train SuperGlue [22] for 2D-3D matching but it cannot be applied to this scale of matching due to the limitation of GPU memory.

TABLE 1

2D-3D feature matching. We report the matching precision (M.Precision), the matching recall (M.Recall), the median positional errors (MPE, no scale), and the median rotation errors (MRE, $^{\circ}$)

Matcher	M.Precision	M.Recall	MPE	MRE
NN+ratio	52.5	28.6	0.493	0.044
NN+cross	36.0	38.0	0.416	0.038
NN+distance	36.7	40.7	0.382	0.036
NN+LGCNet-2D3D	55.0	41.5	0.374	0.036
NN+OANet-2D3D	55.8	42.3	0.364	0.036
GAM	57.0	50.8	0.335	0.030

Results are listed in Table 1. Compared with other handcrafted methods, although NN+ratio has high matching precision, its pose error is the largest in all hand-crafted methods. This is because a large number of correct matches are filtered after ratio test. Some qualitative 2D-3D matches are illustrated in Fig.5. Due to the existence of repetitive patterns, NN+ratio shows few matches compared to other methods. Compared with NN+LGCNet-2D3D, NN+OANet-2D3D is better under various metrics.

The improvement is mainly brought by the usage of the local context of 2D-3D correspondences. GAM has a significantly higher recall than both handcrafted and learned baselines, which can attribute to k NN ratio matching that can recall the true matches that are not in the nearest neighbors. Meanwhile, although GAM takes more ambiguous matches into consideration, it also maintains a higher precision than hand-crafted and learned methods. This is because BMNet equipped with the Hungarian pooling layer has the ability to find out true matches from original many-to-many ambiguous matches. Fig.5 also shows the effectiveness of the proposed matching method GAM.

5.3 Visual Localization

We continue to evaluate the effectiveness of GAM in visual localization and our proposed visual localization framework.

Dataset. We conduct experiments on Aachen Day-Night dataset, which is a challenging large dataset introduced by [61]. The images of Aachen Day-Night dataset consist of two parts, the reference images that are used to construct the sparse SfM model and the query images that are used for evaluation. All query images are annotated with the ground-truth 6DoF poses. Aachen Day-Night [62] contains 4,328 reference images (all captured in the daytime) and 922 query images (824 captured in the daytime and 98 in the nighttime). All the query images are collected using mobile phones, which are very suitable for augmented reality scenes. The light changes during the day and night bring great challenges to visual localization.

Metric. We report the pose recall at different accuracy levels of positions and orientations. We follow the benchmark [61] and use three accuracy levels ($0.25m, 2^{\circ}$), ($0.5m, 5^{\circ}$) and ($5.0m, 10^{\circ}$).

Feature Matching. We first evaluate the effectiveness of GAM in visual localization. In this experiment, we intentionally just use the first scene provided by scene retrieval (SR¹) to perform feature matching. Our focus is on the performance of various matching methods in visual localization. We compare GAM with traditional hand-

crafted methods, including NN+ratio, NN+distance, and NN+cross. We also compare our method with learned methods NN+LGCNet-2D3D and NN+OANet-2D3D as in the 2D-3D matching experiment. At the image retrieval stage, we use NetVLAD [40] to retrieve top-50 images for all matching methods.

TABLE 2

Visual Localization on the Aachen Day-Night datasets. We report the pose recall [%] at different accuracy levels of positions (m) and orientations (deg). **Bold** numbers denote the best result.

Method		Aachen Day-Night	
Coarse	Fine	Day	Night
SR ¹	NN+ratio	79.7 / 88.8 / 93.7	54.1 / 70.4 / 81.6
	NN+cross	83.7 / 90.9 / 94.1	68.4 / 78.6 / 85.7
	NN+distance	82.0 / 90.2 / 94.1	66.3 / 78.6 / 84.7
	NN+LGCNet-2D3D	84.3 / 90.7 / 94.3	69.4 / 78.6 / 88.8
	NN+OANet-2D3D	82.6 / 90.0 / 94.1	67.3 / 77.6 / 85.7
	GAM	84.7 / 91.3 / 94.3	73.5 / 83.7 / 88.8
IR		85.7 / 93.3 / 96.8	73.5 / 86.7 / 93.9
CC	GAM	86.9 / 93.9 / 97.8	76.5 / 88.8 / 95.9
SR		88.0 / 94.8 / 98.5	78.6 / 91.8 / 99.0

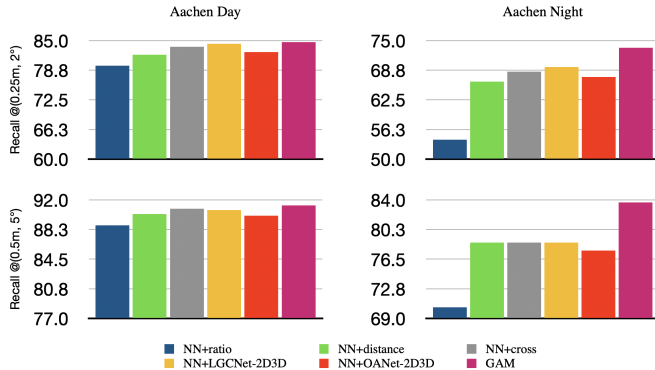


Fig. 6. Pose recall under two high precision thresholds on Aachen Day-Night dataset. GAM consistently outperforms all baseline methods and shows a larger improvement on the night queries than the day.

Results are presented in Table 2. GAM consistently outperforms all hand-crafted and learned baselines on both day and night queries, except at threshold ($5.0m, 10^\circ$), under which GAM shows the same result with NN+LGCNet-2D3D. This confirms that GAM can effectively improve the accuracy of feature-based localization. It is worth noting that the improvement brought by GAM on the night queries is greater than that on the day queries, which is shown in Fig. 6. This is because the discriminative power of appearance is reduced under the condition of severe light changes. In this case, the 2D-3D correspondences established only by finding the nearest neighbor in the descriptor space are not enough to provide accurate camera poses. GAM can effectively alleviate this problem, which shows the advantage of GAM at the complex condition. It should be pointed out that OANet-2D3D performs slightly worse than LGCNet-2D3D. We argue that this might be due to 3D points obtained by scene retrieval in large-scale scenes are not friendly to capturing local geometric context.

Scene Retrieval. We proceed to the evaluation of the proposed visual localization pipeline based on GAM. Our

focus is on the performance of various coarse localization methods. At the image retrieval stage, we use NetVLAD [40] to retrieve top-50 images. We compare the proposed method scene retrieval (SR) with co-visible cluster [7] (CC). At the same time, we directly perform feature matching between the query features and 3D points provided by all retrieved images. We mark this plain method as IR.

Results are shown in Table 2. SR consistently outperforms both IR and CC. This comparison verifies the effectiveness of scene retrieval. The first reason for the improvement brought by scene retrieval is that it provides a cleaner 3D points set that is friendly to capture geometric context for GAM. The second is that scene retrieval is able to recall 3D points that would otherwise be lost due to image retrieval.

5.4 Comparison with State-of-the-art Methods

We now compare our proposed pipeline with state-of-the-arts on both the Cambridge Landmarks dataset and a large-scale long-term localization benchmark.

5.4.1 Cambridge Landmarks

Cambridge Landmarks dataset [47] is commonly used for end-to-end learning methods and contains six medium-scale outdoor scenes. Each scene includes the training images and the test images which are collected on different paths and different conditions. All images have the ground-truth camera poses obtained by SfM. The Street scene is excluded for evaluation due to the errors in the provided trajectory. The remaining five scenes are re-triangulated with SuperPoint feature by HLoc toolbox [60].

We compare our proposed pipeline to end-to-end methods (E2E), including PoseNet [47], DFNet [49], DSAC [51], DSAC++ [52], NG-DSAC [30] and PixLoc [55]. We also compare our method with state-of-the-art feature-based localization methods (FM). Active Search (AS) [2] directly perform feature matching between 2D and 3D (2D3D). HLoc+SuperGlue (HLoc+SG) [1], [22], a state-of-the-art 2D-2D localization method, establishes 2D-3D correspondences by performing 2D-2D feature matching many times (2D2D). We use NetVLAD to retrieve top-10 reference images for HLoc+SG and ours.

Results are presented in Table 3. The results of PoseNet, spatial LSTM, DSAC and DSAC++ come from the paper [52]. The NG-DSAC results are obtained by using the model released by the author. The results of PixLoc and AS come from [55]. The result of HLoc+SG is obtained from our implementation based on the released model by the author. We found that our re-implemented result is better than the author's. As can be seen from Table 3, the methods that regress scene coordinates, such as DSAC, DSAC++, and NG-DSAC, perform better than the methods that directly regress camera pose, such as PoseNet. Our method is more accurate than the methods of regressing scene coordinates and PixLoc. These results indicate that for the complicated task of localization, using the learning in the specific modules may be more effective than learning the whole process. Not only that, but our method also consistently outperforms AS by a large margin in all scenes. Compared with the state-of-the-art 2D-2D localization method, our method outperforms HLoc+SG in all scenes except Great Court. Note that

TABLE 3

Visual localization on the Cambridge Landmarks dataset. We report the median translation (*cm*) and rotation (\circ) errors on five scenes and compute the mean errors. We mark best results **bold**.

Method	Great Court	Kings College	Old Hospital	Shop Facade	St M. Church	Avg
E2E	PoseNet	700cm, 3.7 \circ	99cm, 1.1 \circ	217cm, 2.9 \circ	105cm, 4.0 \circ	149cm, 3.4 \circ
	DFNet	-	43cm, 0.87 \circ	46cm, 0.87 \circ	16cm, 0.59 \circ	50cm, 1.49 \circ
	DSAC	280cm, 1.5 \circ	30cm, 0.5 \circ	33cm, 0.6 \circ	9cm, 0.4 \circ	55cm, 1.6 \circ
	DSAC++	40.3cm, 0.20 \circ	17.7cm, 0.30 \circ	19.6cm, 0.30 \circ	5.7cm, 0.30 \circ	12.5cm, 0.40 \circ
	NG-DASC	34.8cm, 0.18 \circ	12.2cm, 0.23 \circ	21.2cm, 0.45 \circ	5.4cm, 0.29 \circ	9.9cm, 0.31 \circ
	PixLoc	30.0cm, 0.14 \circ	14.0cm, 0.24 \circ	16.0cm, 0.32 \circ	5.0cm, 0.23 \circ	10.0cm, 0.34 \circ
FM(2D2D)	HLoc+SG	10.1cm, 0.07\circ	6.9cm, 0.11 \circ	12.5cm, 0.24 \circ	2.9cm, 0.14 \circ	3.8cm, 0.12 \circ
FM(2D3D)	AS	24.0cm, 0.13 \circ	13.0cm, 0.22 \circ	20.0cm, 0.36 \circ	4.0cm, 0.21 \circ	8.0cm, 0.25 \circ
	Ours	10.6cm, 0.08 \circ	5.4cm, 0.10\circ	11.0cm, 0.22\circ	2.5cm, 0.13\circ	3.5cm, 0.11\circ

TABLE 4

Visual Localization on the Aachen Day-Night and RobotCar Seasons datasets. We report the pose recall [%] at different accuracy levels of positions (*m*) and orientations (*deg*). **Bold** numbers denote the best result. A dash (-) indicates that the result was not reported by the corresponding methods.

Method		Aachen Day-Night		RobotCar Seasons	
Category	Name	Day	Night	Day	Night
E2E	ESAC	42.6 / 59.6 / 75.5	6.1 / 10.2 / 18.4	-	-
	PixLoc	84.6 / 92.4 / 98.2	69.4 / 87.8 / 95.9	56.8 / 81.4 / 98.6	8.8 / 25.6 / 58.2
FM(2D2D)	HLoc+SG	89.6 / 95.4 / 98.8	86.7 / 93.9 / 100.0	56.9 / 81.7 / 98.1	33.3 / 65.9 / 88.8
FM(2D3D)	AS	85.3 / 92.2 / 97.9	39.8 / 49.0 / 64.3	43.6 / 76.0 / 94.0	1.8 / 7.4 / 14.2
	CSL	52.3 / 80.0 / 94.3	29.6 / 40.8 / 56.1	45.3 / 73.5 / 90.1	0.6 / 2.6 / 7.2
	HLoc	80.5 / 87.4 / 94.2	68.4 / 77.6 / 88.8	53.1 / 79.1 / 95.5	7.2 / 17.4 / 34.4
	Ours	88.0 / 94.8 / 98.5	78.6 / 91.8 / 99.0	57.8 / 81.6 / 97.4	12.6 / 35.3 / 69.4

although HLoc+SG has higher accuracy than our method on Great Court, its speed is about 6 times slower than our method, which can be seen in Fig.8.

5.4.2 Large-scale Localization

We compare our method with state-of-the-art methods on the Aachen Day-Night dataset and the RobotCar Seasons dataset. The RobotCar dataset [63] consists of several video sequences collected in different seasons, including 26,121 reference images and 11,934 query images. The reference images from one season are used to construct the SfM model. Compared to Aachen Day-Night, the query images are even more challenging because both seasonal changes and illumination changes are included.

We compare our method with Active Search (AS) [2], City Scale Localization (CSL) [3], HLoc [1] and HLoc+SuperGlue (HLoc+SG) [1], [22]. These methods are based on feature matching (FM). In addition, we compare against end-to-end learning-based methods (E2E), ESAC [64] and PixLoc [55]. We use the results retrieved by NetVLAD, which is the same as HLoc [1]. The evaluation metric follows the benchmark [61].

Results are shown in Table 4. Our method consistently outperforms ESAC and outperforms the recently proposed PixLoc except on the day queries of RobotCar under the threshold (5*m*, 10 \circ). On two datasets, our method also consistently outperforms localization methods based on 2D-3D matching including AS, CSL, and HLoc. It is worth mentioning that every 3D point used in HLoc is represented by all 2D descriptors in the track when performing 2D-3D feature matching, while our method only uses the mean of

these descriptors, which greatly reduces the requirement of storage and timing. This confirms that our method is effective. Compared with the state-of-the-art 2D-2D localization method, although HLoc+SG establishes 2D-3D correspondences by performing 2D-2D feature matching many times, our method performs comparably to HLoc+SG on the Aachen Day-Night dataset and the day queries of RobotCar Seasons dataset. Note that our method is slightly better than HLoc+SG on the day queries of RobotCar Seasons dataset under threshold (0.25*m*, 2 \circ).

5.5 Ablation Study

In this section, we will give ablation studies about our proposed method. We present experiments on the 2D-3D matching dataset. Our focus is on the behaviors of GAM with different configurations.

k-Nearest Neighbors. We evaluate the impact of hyper-parameter *k* in GAM. The ratio threshold is fixed as 0.7, aiming to filter obviously false matches. We have two significant observations from Fig.7. First, with the increase of *k*, the recall increases, and the precision slightly decreases. This indicates that GAM can effectively strengthen the recall of 2D-3D matches while maintaining high precision. Second, with the increase of *k*, both MPE and MAE are dropped first. The median error reaches the minimum at *k* = 3, which is improved by about 13% compared to *k* = 1. When *k* increases, both MPE and MAE fluctuate, but the fluctuation range is small and will not perform worse than when *k* = 1. This verifies the effectiveness of leveraging *k* nearest neighbors.

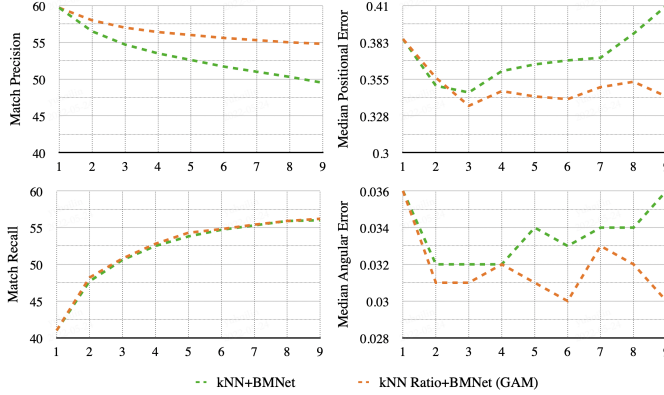


Fig. 7. Match precision (top left), match recall (bottom left), median positional error (top right), and median angular error (bottom right) on the test dataset. Horizontal coordinate represents hyper-parameter k .

kNN vs. kNN Ratio. To demonstrate the effectiveness of k NN ratio, we compare k NN ratio+BMNet (GAM) with k NN+BMNet under various k . The only difference between both methods is the candidate matches fed into BMNet. The results are presented in Fig.7. First, the match recall of both k NN ratio+BMNet and k NN+BMNet are almost identical, but k NN+BMNet has lower match precision than k NN ratio+BMNet. Both the minimum MAP and MPE of k NN+BMNet are larger than that of k NN ratio+BMNet. Second, with the increase of k , both MPE and MAE of k NN+BMNet are dropped first and then increased, which is different from k NN ratio+BMNet which shows fluctuation after reaching the minimum. The MPE of k NN+BMNet at $k = 8$ even exceeds that at $k = 1$. This indicates that k NN ratio+BMNet is less sensitive to k value than k NN+BMNet and shows more robustness.

Hungarian Pooling. We train a model without Hungarian pooling (HP) denoted as PlainNet. We compare PlainNet and PlainNet+HP with BMNet. Hungarian pooling layer is parameter-free, so PlainNet has the same number of parameters as BMNet. The initial candidate 2D-3D matches are generated by k NN ratio matcher for both models. As shown in Table 5, although PlainNet has a higher matching recall than BMNet, it shows lower matching precision and poses accuracy. This indicates that Hungarian pooling is able to filter out geometrically ambiguous matches, which have a negative effect on pose estimation. BMNet also outperforms PlainNet+HP. The only difference between the two methods is that BMNet is trained end-to-end with Hungarian pooling. This comparison verifies the effectiveness of end-to-end training with Hungarian pooling layer.

Negative Sample Mining. We train a model without negative sample mining (mining) denoted as BMNet (w/o mining). When training BMNet (w/o mining), the negative samples are generated by the random selection that is adopted by [23]. The other configurations are kept the same as BMNet. We compare BMNet (w/o mining) with BMNet. The initial candidate 2D-3D matches are obtained by k NN ratio matcher. As shown in Table 5, BMNet outperforms BMNet (w/o mining) under all metrics. This comparison verifies the effectiveness of negative sample mining at the training stage.

TABLE 5
Ablation Study. We report the matching precision (M.Precision), the matching recall (M.Recall), the median positional errors (MPE, no scale), and the median rotation errors (MRE, $^{\circ}$). The candidate matches are obtained by kNN ratio

Matcher	M.Precision	M.Recall	MPE	MRE
PlainNet	16.7	62.8	0.471	0.044
PlainNet+HP	53.6	49.2	0.372	0.036
BMNet (w/o mining)	55.2	50.1	0.342	0.032
BMNet	57.0	50.8	0.335	0.030

5.6 Timing

We measure the running time of the main components of the proposed method on the machine with an Intel Core i7-8700 CPU and a GeForce GTX 1080 GPU. We resize the larger dimension of the query images to 1024 for SuperPoint and NetVLAD. We calculate the average running time on the Great Court scene of Cambridge Landmarks dataset [47]. The scene includes 153,2 reference images and 760 query images. The run-time of main components are presented in Table 6. The average number of processed scenes on this dataset is 1.06, so the average time of the whole pipeline is 309.59ms. The details about the running time of BMNet used in GAM can be seen in Fig.8(a). The sizes of the 2D point set and 3D point set are equal and the size of the edge set is twice as much as the size of the 2D point set. BMNet takes 39.39ms and 62.4ms when the point set size is 512 and 1024, respectively.

TABLE 6
Running Time. We report the mean run-time (ms) of different components of the proposed localization method. SP and NV represent SuperPoint and NetVLAD. SR represents scene retrieval. PE represents prior-guided pose estimation.

Component	SP	NV	SR	GAM	PE
Times(ms)	35.33	80.62	14.62	117.43	50.63

The Number of Retrieved Images. We conduct more studies about the relationship between the median positional error and running time with the number of retrieved images. We present the results of our method and HLoc+SG [22] in Fig.8(b)(c)(d). Note the time of extracting SuperPoint and NetVLAD is excluded here. The elapsed time of our method is insensitive to the number of retrieved images, while the elapsed time of HLoc+SG is linearly related to the number of retrieved images. In addition, HLoc+SG is more dependent on the number of retrieved images than our method in terms of pose accuracy. Although HLoc+SG is slightly accurate than ours as the number of retrieved images increases to 10, it takes more than six times as long as ours.

5.7 Application for Augmented Reality

Global localization with 6DoF pose estimation is crucial for augmented reality applications in a large-scale scene. In this section, we use the proposed visual localization method to make an AR application.

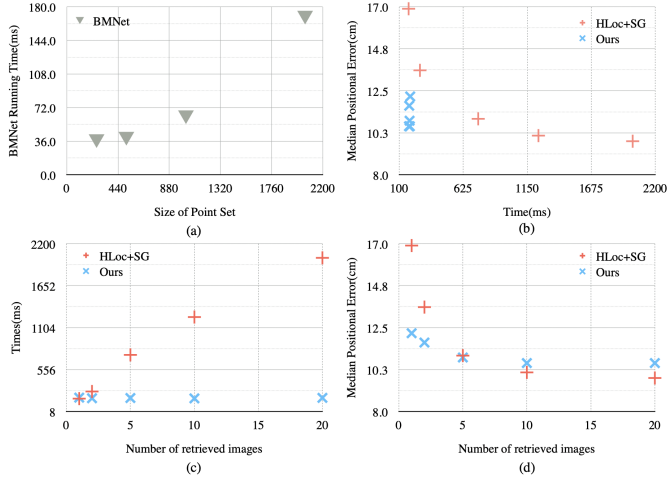


Fig. 8. (a) Running time of BMNet with various sizes of the point set. (b) The relationship between median positional error and elapsed time with various the number of retrieved images. (c) The relationship between elapsed time and the number of retrieved images. (d) The relationship between median positional error and the number of retrieved images.

We capture a video in an office covering about 1,000 square meters. We extract frames from this video as reference images that are used to reconstruct a sparse SfM model with SuperPoint. Then we choose some locations to place some virtual 3D arrows. The coordinates of these virtual objects are aligned to the SfM model.

We capture a query video and extract frames from the query video at 30 fps. To demonstrate the accuracy and robustness of our localization result, we use the proposed localization method to recover the camera poses for all frames. Then we render the pre-aligned virtual objects on these frames according to the localization results. Some AR frames are shown in Fig. 9. The recovered camera trajectory is shown in Fig. 10. It can be seen that the recovered trajectory by our method is already quite smooth even the pose of each frame is estimated independently. All the poses of all frames are faithfully recovered, which demonstrates the effectiveness of the proposed visual localization method. Please refer to the supplementary video for watching the whole result.

Actually, for AR application, we do not need to estimate the pose of each frame independently by global relocalization, since SLAM [65], [66] technique can be used to smoothly recover the poses of each online frame. Global relocalization can be used to align the 3D coordinate of SLAM into the world coordinate and correct the pose to eliminate tracking drift.

In this application, we use ARkit¹ to recover the camera pose in real-time. We first use the proposed localization to align ARkit results to SfM coordinate. Then the localization and alignment are performed every 10 seconds. Please refer to the supplementary video for watching the AR effect. Since our main focus is on visual localization, we use this simple strategy to couple SLAM and global localization results. Some more effective couple methods can be referred to [67], [68], [69], [70].

1. <https://developer.apple.com/augmented-reality/arkit>

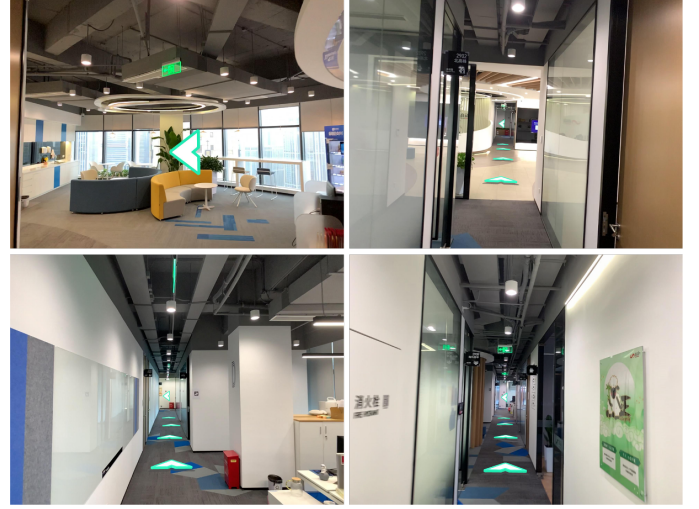


Fig. 9. Four selected augmented frames. The arrows on the ground and in the air are pre-aligned virtual objects.

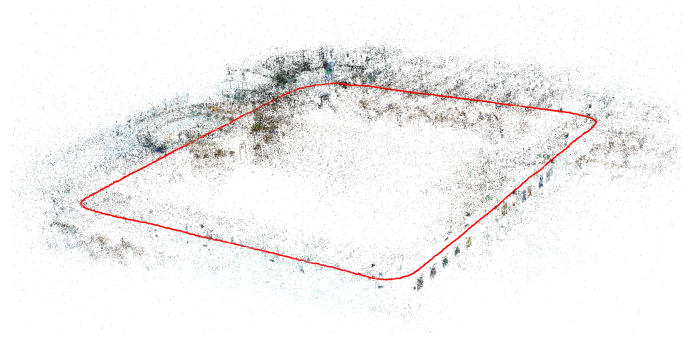


Fig. 10. The recovered camera trajectory superimposed in the offline 3D map recovered by SfM. All poses are faithfully recovered.

6 CONCLUSION

This paper proposes an effective 2D-3D matching method GAM for visual localization. GAM uses both the appearance information and geometric context to improve the matching performance, which greatly improves the recall of 2D-3D matching while maintaining high precision. GAM introduces a novel bipartite matching neural network BMNet to extracts geometric features for a set of 2D-3D correspondences and can learn the global geometric consistency to predict the possibility of being a true match for each correspondence. GAM also integrates the Hungarian algorithm into BMNet as a special pooling layer to find maximum-weight matching in an end-to-end manner. This approach enables the localization to obtain more correct matches and hence improves the robustness and accuracy of localization. We further combine GAM with a novel scene retrieval strategy and propose a new hierarchical localization method. Extensive experiments show that the proposed method achieves the state-of-the-art results on multiple datasets.

ACKNOWLEDGMENTS

This work was partially supported by NSF of China (Nos.61932003 and 61822310).

REFERENCES

- [1] P.-E. Sarlin, C. Cadena, R. Siegwart, and M. Dymczyk, "From Coarse to Fine: Robust Hierarchical Localization at Large Scale," in *Proceedings of the IEEE Conference on Computer Vision and Pattern Recognition*, 2019, pp. 12 716–12 725.
- [2] T. Sattler, B. Leibe, and L. Kobbelt, "Improving image-based localization by active correspondence search," in *ECCV*. Springer, 2012, pp. 752–765.
- [3] L. Svärm, O. Enqvist, F. Kahl, and M. Oskarsson, "City-scale localization for cameras with known vertical direction," *IEEE Transactions on Pattern Analysis and Machine Intelligence*, vol. 39, no. 7, pp. 1455–1461, 2016.
- [4] L. Liu, H. Li, and Y. Dai, "Efficient global 2D-3D matching for camera localization in a large-scale 3D map," in *Proceedings of the IEEE International Conference on Computer Vision*, 2017, pp. 2372–2381.
- [5] Y. Li, N. Snavely, and D. P. Huttenlocher, "Location recognition using prioritized feature matching," in *ECCV*. Springer, 2010, pp. 791–804.
- [6] B. Zeisl, T. Sattler, and M. Pollefeys, "Camera pose voting for large-scale image-based localization," in *Proceedings of the IEEE International Conference on Computer Vision*, 2015, pp. 2704–2712.
- [7] P.-E. Sarlin, F. Debraine, M. Dymczyk, R. Siegwart, and C. Cadena, "Leveraging deep visual descriptors for hierarchical efficient localization," in *Conference on Robot Learning*. PMLR, 2018, pp. 456–465.
- [8] H. Taira, M. Okutomi, T. Sattler, M. Cimpoi, M. Pollefeys, J. Sivic, T. Pajdla, and A. Torii, "InLoc: Indoor visual localization with dense matching and view synthesis," in *Proceedings of the IEEE Conference on Computer Vision and Pattern Recognition*, 2018, pp. 7199–7209.
- [9] L. Kneip, D. Scaramuzza, and R. Siegwart, "A novel parametrization of the perspective-three-point problem for a direct computation of absolute camera position and orientation," in *Proceedings of the IEEE Conference on Computer Vision and Pattern Recognition*. IEEE, 2011, pp. 2969–2976.
- [10] V. Lepetit, F. Moreno-Noguer, and P. Fua, "EPnP: An accurate O(N) solution to the PnP problem," *International journal of computer vision*, vol. 81, no. 2, p. 155, 2009.
- [11] M. A. Fischler and R. C. Bolles, "Random Sample Consensus: a paradigm for model fitting with applications to image analysis and automated cartography," *Communications of the ACM*, vol. 24, no. 6, pp. 381–395, 1981.
- [12] D. G. Lowe, "Distinctive image features from scale-invariant keypoints," *International Journal of Computer Vision*, vol. 60, no. 2, pp. 91–110, 2004.
- [13] Z. Luo, T. Shen, L. Zhou, J. Zhang, Y. Yao, S. Li, T. Fang, and L. Quan, "ContextDesc: Local descriptor augmentation with cross-modality context," in *Proceedings of the IEEE Conference on Computer Vision and Pattern Recognition*, 2019, pp. 2527–2536.
- [14] Y. Tian, X. Yu, B. Fan, F. Wu, H. Heijnen, and V. Balntas, "SOSNet: Second order similarity regularization for local descriptor learning," in *Proceedings of the IEEE Conference on Computer Vision and Pattern Recognition*, 2019, pp. 11 016–11 025.
- [15] Z. Luo, T. Shen, L. Zhou, S. Zhu, R. Zhang, Y. Yao, T. Fang, and L. Quan, "GeoDesc: Learning local descriptors by integrating geometry constraints," in *ECCV*, 2018, pp. 168–183.
- [16] K. M. Yi, E. Trulls, V. Lepetit, and P. Fua, "Lift: Learned invariant feature transform," in *ECCV*. Springer, 2016, pp. 467–483.
- [17] D. DeTone, T. Malisiewicz, and A. Rabinovich, "SuperPoint: Self-supervised interest point detection and description," in *Proceedings of the IEEE Conference on Computer Vision and Pattern Recognition Workshops*, 2018, pp. 224–236.
- [18] M. Dusmanic, I. Rocco, T. Pajdla, M. Pollefeys, J. Sivic, A. Torii, and T. Sattler, "D2-Net: A trainable CNN for joint description and detection of local features," in *Proceedings of the IEEE/cvf conference on computer vision and pattern recognition*, 2019, pp. 8092–8101.
- [19] K. Moo Yi, E. Trulls, Y. Ono, V. Lepetit, M. Salzmann, and P. Fua, "Learning to find good correspondences," in *Proceedings of the IEEE Conference on Computer Vision and Pattern Recognition*, 2018, pp. 2666–2674.
- [20] J. Zhang, D. Sun, Z. Luo, A. Yao, L. Zhou, T. Shen, Y. Chen, L. Quan, and H. Liao, "Learning two-view correspondences and geometry using order-aware network," in *Proceedings of the IEEE International Conference on Computer Vision*, 2019, pp. 5845–5854.
- [21] F. Xue, I. Budvytis, D. O. Reino, and R. Cipolla, "Efficient large-scale localization by global instance recognition," in *Proceedings of the IEEE/CVF Conference on Computer Vision and Pattern Recognition*, 2022, pp. 17 348–17 357.
- [22] P.-E. Sarlin, D. DeTone, T. Malisiewicz, and A. Rabinovich, "SuperGlue: Learning feature matching with graph neural networks," in *Proceedings of the IEEE/CVF conference on computer vision and pattern recognition*, 2020, pp. 4938–4947.
- [23] H. Yu, W. Ye, Y. Feng, H. Bao, and G. Zhang, "Learning bipartite graph matching for robust visual localization," in *2020 IEEE International Symposium on Mixed and Augmented Reality (ISMAR)*. IEEE, 2020, pp. 146–155.
- [24] E. Rublee, V. Rabaud, K. Konolige, and G. Bradski, "ORB: An efficient alternative to SIFT or SURF," in *2011 International Conference on Computer Vision*. IEEE, 2011, pp. 2564–2571.
- [25] J. Bian, W.-Y. Lin, Y. Matsushita, S.-K. Yeung, T.-D. Nguyen, and M.-M. Cheng, "Gms: Grid-based motion statistics for fast, ultra-robust feature correspondence," in *Proceedings of the IEEE Conference on Computer Vision and Pattern Recognition*, 2017, pp. 4181–4190.
- [26] J. Ma, J. Zhao, J. Jiang, H. Zhou, and X. Guo, "Locality preserving matching," *International Journal of Computer Vision*, vol. 127, no. 5, pp. 512–531, 2019.
- [27] O. Chum and J. Matas, "Matching with PROSAC-progressive sample consensus," in *2005 IEEE Computer Society Conference on Computer Vision and Pattern Recognition*, vol. 1. IEEE, 2005, pp. 220–226.
- [28] O. Chum, J. Matas, and J. Kittler, "Locally optimized RANSAC," in *Joint Pattern Recognition Symposium*. Springer, 2003, pp. 236–243.
- [29] D. Barath and J. Matas, "Graph-cut RANSAC," in *Proceedings of the IEEE Conference on Computer Vision and Pattern Recognition*, 2018, pp. 6733–6741.
- [30] E. Brachmann and C. Rother, "Neural-guided RANSAC: Learning where to sample model hypotheses," in *Proceedings of the IEEE International Conference on Computer Vision*, 2019, pp. 4322–4331.
- [31] I. Rocco, M. Cimpoi, R. Arandjelović, A. Torii, T. Pajdla, and J. Sivic, "Neighbourhood consensus networks," *Advances in neural information processing systems*, vol. 31, 2018.
- [32] D. F. Crouse, "On implementing 2D rectangular assignment algorithms," *IEEE Transactions on Aerospace and Electronic Systems*, vol. 52, no. 4, pp. 1679–1696, 2016.
- [33] H. W. Kuhn, "The Hungarian method for the assignment problem," *Naval Research Logistics Quarterly*, vol. 2, no. 1-2, pp. 83–97, 1955.
- [34] T. S. Caetano, J. J. McAuley, L. Cheng, Q. V. Le, and A. J. Smola, "Learning graph matching," *IEEE Transactions on Pattern Analysis and Machine Intelligence*, vol. 31, no. 6, pp. 1048–1058, 2009.
- [35] A. Zanfir and C. Sminchisescu, "Deep learning of graph matching," in *Proceedings of the IEEE Conference on Computer Vision and Pattern Recognition*, 2018, pp. 2684–2693.
- [36] Y. Shi, J.-X. Cai, Y. Shavit, T.-J. Mu, W. Feng, and K. Zhang, "Clustergnn: Cluster-based coarse-to-fine graph neural network for efficient feature matching," in *Proceedings of the IEEE/CVF Conference on Computer Vision and Pattern Recognition*, 2022, pp. 12 517–12 526.
- [37] J. Sun, Z. Wang, S. Zhang, X. He, H. Zhao, G. Zhang, and X. Zhou, "Onepose: One-shot object pose estimation without cad models," in *Proceedings of the IEEE/CVF Conference on Computer Vision and Pattern Recognition*, 2022, pp. 6825–6834.
- [38] T. Sattler, M. Havlena, F. Radenovic, K. Schindler, and M. Pollefeys, "Hyperpoints and fine vocabularies for large-scale location recognition," in *Proceedings of the IEEE International Conference on Computer Vision*, 2015, pp. 2102–2110.
- [39] T. Sattler, B. Leibe, and L. Kobbelt, "Fast image-based localization using direct 2D-to-3D matching," in *2011 International Conference on Computer Vision*. IEEE, 2011, pp. 667–674.
- [40] R. Arandjelovic, P. Gronat, A. Torii, T. Pajdla, and J. Sivic, "NetVLAD: CNN architecture for weakly supervised place recognition," in *Proceedings of the IEEE Conference on Computer Vision and Pattern Recognition*, 2016, pp. 5297–5307.
- [41] A. Torii, R. Arandjelovic, J. Sivic, M. Okutomi, and T. Pajdla, "24/7 place recognition by view synthesis," in *Proceedings of the IEEE Conference on Computer Vision and Pattern Recognition*, 2015, pp. 1808–1817.
- [42] J. Knopp, J. Sivic, and T. Pajdla, "Avoiding confusing features in place recognition," in *ECCV*. Springer, 2010, pp. 748–761.
- [43] T. Naseer, G. L. Oliveira, T. Brox, and W. Burgard, "Semantics-aware visual localization under challenging perceptual condi-

tions," in *2017 IEEE International Conference on Robotics and Automation*. IEEE, 2017, pp. 2614–2620.

[44] C. Toft, E. Stenborg, L. Hammarstrand, L. Brynte, M. Pollefeys, T. Sattler, and F. Kahl, "Semantic match consistency for long-term visual localization," in *ECCV*, 2018, pp. 383–399.

[45] S. Brahmbhatt, J. Gu, K. Kim, J. Hays, and J. Kautz, "Geometry-aware learning of maps for camera localization," in *Proceedings of the IEEE Conference on Computer Vision and Pattern Recognition*, 2018, pp. 2616–2625.

[46] F. Walch, C. Hazirbas, L. Leal-Taixé, T. Sattler, S. Hilsenbeck, and D. Cremers, "Image-based localization using lstms for structured feature correlation," in *Proceedings of the IEEE International Conference on Computer Vision*, 2017, pp. 627–637.

[47] A. Kendall, M. Grimes, and R. Cipolla, "PoseNet: A convolutional network for real-time 6-DoF camera relocalization," in *Proceedings of the IEEE International Conference on Computer Vision*. IEEE, 2015, pp. 2938–2946.

[48] Y. Shavit and Y. Keller, "Camera pose auto-encoders for improving pose regression," in *European Conference on Computer Vision*. Springer, 2022, pp. 140–157.

[49] S. Chen, X. Li, Z. Wang, and V. A. Prisacariu, "Dfnet: Enhance absolute pose regression with direct feature matching," *arXiv preprint arXiv:2204.00559*, 2022.

[50] J. Shotton, B. Glocker, C. Zach, S. Izadi, A. Criminisi, and A. Fitzgibbon, "Scene coordinate regression forests for camera relocalization in RGB-D images," in *Proceedings of the IEEE Conference on Computer Vision and Pattern Recognition*, 2013, pp. 2930–2937.

[51] E. Brachmann, A. Krull, S. Nowozin, J. Shotton, F. Michel, S. Gumhold, and C. Rother, "DSAC-differentiable RANSAC for camera localization," in *Proceedings of the IEEE Conference on Computer Vision and Pattern Recognition*, 2017, pp. 6684–6692.

[52] E. Brachmann and C. Rother, "Learning less is more-6d camera localization via 3D surface regression," in *Proceedings of the IEEE Conference on Computer Vision and Pattern Recognition*, 2018, pp. 4654–4662.

[53] X. Wu, H. Zhao, S. Li, Y. Cao, and H. Zha, "Sc-wls: Towards interpretable feed-forward camera re-localization," in *European Conference on Computer Vision*. Springer, 2022, pp. 585–601.

[54] T. Sattler, Q. Zhou, M. Pollefeys, and L. Leal-Taixé, "Understanding the limitations of CNN-based absolute camera pose regression," in *Proceedings of the IEEE Conference on Computer Vision and Pattern Recognition*, 2019, pp. 3302–3312.

[55] P.-E. Sarlin, A. Unagar, M. Larsson, H. Germain, C. Toft, V. Larsson, M. Pollefeys, V. Lepetit, L. Hammarstrand, F. Kahl *et al.*, "Back to the feature: Learning robust camera localization from pixels to pose," in *Proceedings of the IEEE/CVF Conference on Computer Vision and Pattern Recognition*, 2021, pp. 3247–3257.

[56] T. Hastie, R. Tibshirani, and J. Friedman, *The elements of statistical learning: data mining, inference, and prediction*. Springer Science & Business Media, 2009.

[57] A. Paszke, S. Gross, F. Massa, A. Lerer, J. Bradbury, G. Chanan, T. Killeen, Z. Lin, N. Gimelshein, L. Antiga *et al.*, "Pytorch: An imperative style, high-performance deep learning library," *Advances in neural information processing systems*, vol. 32, pp. 8026–8037, 2019.

[58] Z. Li and N. Snavely, "Megadepth: Learning single-view depth prediction from internet photos," in *Proceedings of the IEEE Conference on Computer Vision and Pattern Recognition*, 2018, pp. 2041–2050.

[59] J. L. Schonberger and J.-M. Frahm, "Structure-from-motion revisited," in *Proceedings of the IEEE Conference on Computer Vision and Pattern Recognition*, 2016, pp. 4104–4113.

[60] P.-E. Sarlin, "The hierarchical localization toolbox," <https://github.com/cvg/Hierarchical-Localization>.

[61] T. Sattler, W. Maddern, C. Toft, A. Torii, L. Hammarstrand, E. Stenborg, D. Safari, M. Okutomi, M. Pollefeys, J. Sivic *et al.*, "Benchmarking 6dof outdoor visual localization in changing conditions," in *Proceedings of the IEEE Conference on Computer Vision and Pattern Recognition*, 2018, pp. 8601–8610.

[62] T. Sattler, T. Weyand, B. Leibe, and L. Kobbelt, "Image retrieval for image-based localization revisited," in *BMVC*, vol. 1, no. 2, 2012, pp. 1–12.

[63] W. Maddern, G. Pascoe, C. Linegar, and P. Newman, "1 year, 1000 km: The oxford robotcar dataset," *The International Journal of Robotics Research*, vol. 36, no. 1, pp. 3–15, 2017.

[64] E. Brachmann and C. Rother, "Expert sample consensus applied to camera re-localization," in *Proceedings of the IEEE/CVF International Conference on Computer Vision*, 2019, pp. 7525–7534.

[65] G. Klein and D. Murray, "Parallel tracking and mapping for small AR workspaces," in *2007 6th IEEE and ACM International Symposium on Mixed and Augmented Reality*. IEEE, 2007, pp. 225–234.

[66] R. Mur-Artal, J. M. M. Montiel, and J. D. Tardos, "ORB-SLAM: a versatile and accurate monocular SLAM system," *IEEE Transactions on Robotics*, vol. 31, no. 5, pp. 1147–1163, 2015.

[67] S. Lynen, T. Sattler, M. Bosse, J. A. Hesch, M. Pollefeys, and R. Siegwart, "Get out of my lab: Large-scale, real-time visual-inertial localization," in *Robotics: Science and Systems*, vol. 1, 2015, p. 1.

[68] X. Zuo, P. Geneva, Y. Yang, W. Ye, Y. Liu, and G. Huang, "Visual-inertial localization with prior lidar map constraints," *IEEE Robotics and Automation Letters*, vol. 4, no. 4, pp. 3394–3401, 2019.

[69] M. Yamaguchi, S. Mori, H. Saito, S. Yachida, and T. Shibata, "Global-map-registered local visual odometry using on-the-fly pose graph updates," in *International Conference on Augmented Reality, Virtual Reality and Computer Graphics*. Springer, 2020, pp. 299–311.

[70] H. Bao, W. Xie, Q. Qian, D. Chen, S. Zhai, N. Wang, and G. Zhang, "Robust tightly-coupled visual-inertial odometry with pre-built maps in high latency situations," *IEEE Trans. Vis. Comput. Graph.*, vol. 28, no. 5, pp. 2212–2222, 2022.